

Vacuum Tribological Properties of Ti-20Zr-6.5Al-4V Alloy as Influenced by Sliding Velocities



H. ZHONG, L.Y. DAI, Y.J. YANG, Y. YUE, B.A. WANG, X.Y. ZHANG, M.Z. MA, and R.P. LIU

This research studied the vacuum tribological properties of annealed Ti-20Zr-6.5Al-4V alloy sliding against AISI 440C steel at various velocities ranging from 0.39 to 1.17 m/s using a ball-on-disc tribometer equipped with a vacuum chamber. The coefficient of friction and wear volumes of the annealed Ti-20Zr-6.5Al-4V alloy were obtained. Results indicated that the coefficient of friction increased at the beginning as the sliding velocity increased to 0.78 m/s and subsequently decreased with further increase in velocity. However, the wear volume increased monotonically with sliding velocity. Scanning electron microscopy was employed to study the wear mechanisms after tribological tests. Under a normal load of 10 N, abrasive wear was predominant at various sliding velocities, whereas the sliding velocity influenced the wear mechanisms significantly when the normal load was increased to 30 N. Under higher normal load, the abrasive wear was indentified as the main wear mechanism at a lower sliding velocity of 0.39 m/s. As the sliding velocity was increased to 1.17 m/s, severer abrasive wear, delamination wear, and plastic deformation were dominant. In addition, at a sliding velocity of 1.17 m/s, the wear mechanisms were abrasive and mild adhesive wear of the TiZrAlV alloy annealed at 1273 K (1000 °C) under the load of 10 N. The mechanism changed to severe plastic deformation and delamination wear when the normal load was increased to 30 N. The three-dimensional topography of the Ti-20Zr-6.5Al-4V disc worn surface was also explored.

DOI: 10.1007/s11661-017-4301-9

© The Minerals, Metals & Materials Society and ASM International 2017

I. INTRODUCTION

THE tribological behaviors for certain materials are extrinsic, and depend on several factors, such as counterpart materials,^[1,2] ambient temperature,^[3,4] normal load,^[5,6] and sliding distance.^[7] Moreover, sliding velocity also significantly influences the tribological performance of various materials.^[8] Asadi Kouhanjani *et al.* investigated the effect of sliding velocity on the friction and wear behavior of Cu-0.65 wt pct Cr alloy and concluded that the Coefficient Friction (COF) and wear loss are sensitive to sliding velocity.^[9] Zhong *et al.* researched the tribological properties of nitrided AISI 4340 steel under various sliding velocities, and the results showed that the COF decreases with increasing sliding velocity for a certain normal load.^[10] Tao *et al.* reported that the sliding velocities apparently affected the COF and wear mechanisms of Zr-based bulk metallic glass.^[11] Straffelini *et al.* investigated the

influence of the counter surface on the dry sliding wear of the Ti-6Al-4V alloy under different friction parameters,^[12] and the results showed that oxidation wear appeared at low sliding velocities and delamination wear at high velocities regardless of the applied load and counter surface.

Ti-based alloys have been widely used as structural material in aerospace, such as in landing gear^[13] and aero-engines,^[14] owing to its high strength-to-density ratio.^[15] Thus, the tribological properties attracted considerable research attention. Molinari *et al.*^[16] conducted disc-on-disc sliding tests with self-mated Ti-6Al-4V alloy under different normal loads and sliding speeds, highlighting that the wear mechanisms were responsible for wear resistance. Qu *et al.*^[17] reported that large frictional fluctuations occurred when metal and ceramic balls were used as counterfaces, whereas the friction coefficient became steady when the polymer ball was used. Chelliah *et al.*^[18] studied the synergy between tribo-oxidation and strain rates of commercial pure titanium during wear and conducted that sliding speeds influenced wear rates through the generated frictional heat. Li *et al.*^[8] investigated the dry sliding wear behavior of the Ti-6.5Al-3.5Mo-1.5Zr-0.3Si alloy and concluded that a severe-to-mild wear transition occurred with the climax at 2.68 m/s at the normal load of 50 N.

H. ZHONG, L.Y. DAI, Y.J. YANG, Y. YUE, B.A. WANG, X.Y. ZHANG, M.Z. MA, and R.P. LIU are with the State Key Laboratory of Metastable Materials Science and Technology, Yanshan University, Qinhuangdao 066004, China. Contact e-mail: mz550509@ysu.edu.cn

Manuscript submitted December 19, 2016.

Article published online August 23, 2017

Owing to the development of aerospace industry, the high strength-to-density Ti prompted further interest in exploring the friction and wear performance of Ti-based alloys as bearing materials.^[19] In the recent decades, an increasing number of new materials were developed to meet the specific demands of serving under the harsh conditions. To this end, a new type of TiZrAlV alloy with a nominal chemical composition of Ti-20Zr-6.5Al-4V (wt pct) was developed by our research group.^[20] Given that Ti and Zr belong to the same subgroup (IVB) in the periodic table and exhibit similar physicochemical properties, large quantities of solution hardening are possible. The Ti-20Zr-6.5Al-4V alloy possessed a high yield strength (exceeding 1000 MPa) with favorable elongation (up to 13 pct),^[21] as well as excellent corrosion-resistance.^[22] These enhanced properties could make the Ti-20Zr-6.5Al-4V alloy a potential candidate for the production of a variety of components for aerospace applications. In the previous research, the main focus of the TiZrAlV alloy was on the material design, microstructure evolution, and mechanical properties.^[20,21,23,24] However, the tribological behavior of the Ti-20Zr-6.5Al-4V alloy was rarely researched. The tribological properties of various materials differ from one another. Furthermore, the space tribology always exists in satellites and spacecrafts; tribological properties under vacuum are critical and should be taken into consideration.^[25]

In the present study, tribological tests on annealed Ti-20Zr-6.5Al-4V alloy were conducted on a ball-on-disc tribometer sliding against AISI 440C steel with various sliding velocities ranging from 0.39 to 1.17 m/s in vacuum. AISI 440C steel was selected as the counterpart material because of the following: (i) steel was typically used as counterpart material in the Ti-based alloy dry sliding tribology system^[26,27]; (ii) AISI 440C is a type of bearing material. For investigating the tribological behavior of the Ti-20Zr-6.5Al-4V alloy as bearing materials, the AISI 440C steel ball was selected as the counterpart. The obtained tribological properties of the annealed Ti-20Zr-6.5Al-4V alloy at various sliding velocities were preliminarily evaluated to determine the tribological behavior of the Ti-20Zr-6.5Al-4V alloy. This research could be used to create a foundation for the potential applications of this alloy in the aerospace industry.

II. EXPERIMENTAL PROCEDURES

The Ti-20Zr-6.5Al-4V alloy rods of 45 mm diameter and 0.5 m length were used as disc material in this study.

Details on the preparation processes and parameters of the Ti-20Zr-6.5Al-4V alloy were presented in the previous literature.^[20] The initial Ti-20Zr-6.5Al-4V alloy rods with a hardness of 40-42 HRC were cut into rods of 0.2 m length through wire-cut electrical discharge machining and subsequently annealed at 1073 K, 1173 K, and 1273 K (that is, 800 °C, 900 °C and 1000 °C) for 90 minutes in a vacuum tube furnace under a protective atmosphere of argon. Then the Ti-20Zr-6.5Al-4V rods were cooled to room temperature in the furnace. The annealing temperature was selected according to the Differential Scanning Calorimetry (DSC) data for the Ti-20Zr-6.5Al-4V alloy, indicating that α to $\alpha + \beta$ and $\alpha + \beta$ to β transus temperatures are 1062 K and 1249 K (789 °C and 976 °C), respectively. Optical Microscopy (OM) Axiovert 200 MAT was used for the microstructure analysis of annealed Ti-20Zr-6.5Al-4V alloy after being etched by Kroll's solution (5 pct HF, 15 pct HNO₃ and 80 pct H₂O). The crystal structures of the annealed samples were analyzed by an X-ray Diffractometer (XRD) Rikagu D/Max 2000 utilizing Cu K _{α} radiation.

Dry sliding tests were performed with a ball-on-disc servo-controlled tribometer equipped with a vacuum chamber (Rtec instruments, MFT 5000). The Ti-20Zr-6.5Al-4V disc geometry was according to the ASTM test method G99-05,^[28] and carefully machined to the dimensions of 45 mm (diameter) \times 4 mm (length). The surface finish of the TiZrAlV discs was ground to the same roughness (0.2 to 0.3 μ m) to exclude the roughness effect on the tribological properties. AISI 440C steel balls with diameter of 9.5 mm and hardness of 55 HRC were used as counterparts. The detailed dry sliding parameters are summarized in Table I. The tribological parameters were selected in this study because of two reasons: First, according to the pin-on-disc test method G99-05; and second, research studies on the tribological properties of the Ti-20Zr-6.5Al-4V alloy were limited. Thus, the present study aimed to provide basic data for future applications. As a consequence, the parameters referred to the other references on tribological test of Ti-6Al-4V or Ti-6.5Al-3.5Mo-1.5Zr-0.3Si alloy.^[29,30] During the sliding tests, the Ti-20Zr-6.5Al-4V alloy disc was rotary, while the upper AISI 440C ball was kept still. The sliding tests were stopped when the sliding distances reached 1700 m. The tribometer was equipped with two sensors to measure the normal force and the frictional force, respectively. The COF was calculated by the frictional force divided by normal force.

After friction and wear tests, the samples were carefully cleaned with alcohol in the ultrasonic cleaner and dried in air. An electronic balance with an accuracy of 10⁻⁴ g was used to measure the weight of the

Table I. Summary of Vacuum Tribological Tests Parameters

Parameters	Unit	Value(s)
Pressure	Pa	6.67×10^{-3}
Annealed Temperature	K (°C)	1073 (800), 1173 (900), 1273 (1000)
Sliding Velocity	m/s	0.39, 0.59, 0.78, 0.98, 1.17
Sliding Distance	m	1700
Normal Load	N	10, 20, 30

Ti-20Zr-6.5Al-4V alloy discs before and after the sliding tests to calculate the wear volume loss. The wear volumes of the disc samples were calculated as the wear weight loss divided by density (4.82 g/cm^3). The average data of the tribological properties were obtained from at least three repeated tests. Scanning Electron Microscopy (SEM) Hitachi 3400N was employed for wear scar analysis on the sample surfaces for the determination of the wear mechanisms. A Three-Dimensional (3D)

optical profilometer was used to characterize the topographies of wear scars. The profilometer provided the color contour with peaks and valleys of the worn surface to illustrate the groove variations on the worn surface with the variations of the sliding velocity.^[31] The interferograms of the wear traces were captured at $10\times$ objective using white light.

III. RESULTS AND DISCUSSION

A. Phase and Microstructure Analyses

The phase constituents of the Ti-20Zr-6.5Al-4V alloy subjected to various annealing temperatures are compared in Figure 1. As shown in the XRD curves, no other phases or intermetallics could be detected except for a large amount of α phase and a relatively less β phase (based on the theory of the peaks corresponding to each phase in multi-phase alloys correlating with the mass percentage of the phase^[32]), displaying that only solid solution phases were formed in the alloy.

Microstructures of the annealed Ti-20Zr-6.5Al-4V alloy are presented in Figure 2. Figure 2(a) shows the microstructures after being annealed at 1073 K (800 °C), as well as a chaotic arrangement of slender α laths and β plates, which were commonly known as a typical Widmanstätten morphology. As the annealing temperature increased, the slender α phase became thicker and shorter (Figures 2(b) through (c)). The trend line of the Length (L) vs Width (W) of α lath after being annealed at different

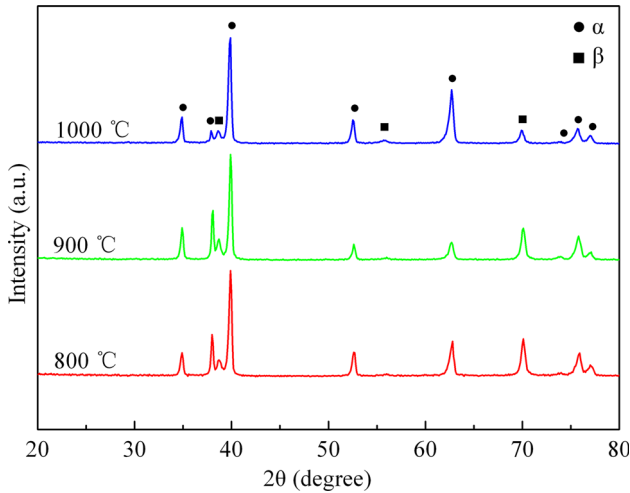


Fig. 1—XRD patterns of annealed Ti-20Zr-6.5Al-4V alloy under different temperatures.

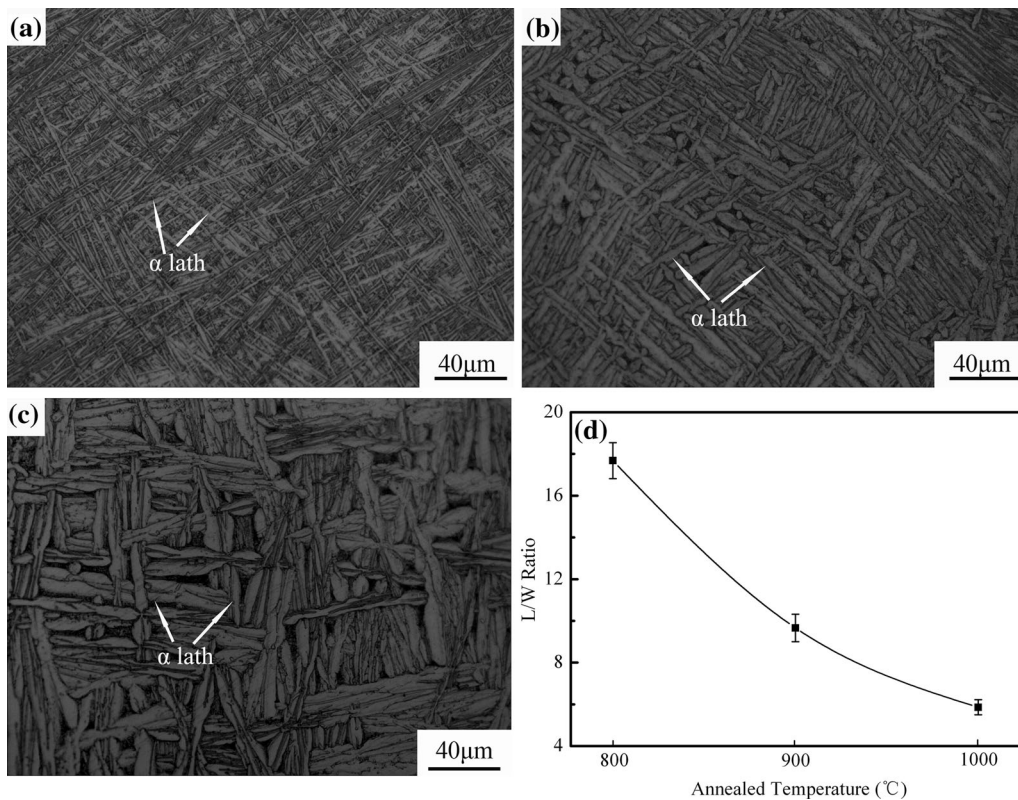


Fig. 2—Optical micrograph of annealed Ti-20Zr-6.5Al-4V at (a) 1073 K (800 °C), (b) 1173 K (900 °C), and (c) 1273 K (1000 °C); (d) shows L/W ratio of the α lath varied with different annealing temperature.

temperatures is expressed in Figure 2(d). From Figure 2(d), a ratio of approximately 18 is obtained after being annealed at 1073 K (800 °C) and then decreased with increasing annealing temperature. At the annealing temperature of 1273 K (1000 °C), the L/W ratio was at the minimum. With increasing annealing temperature, the L/W ratio of α lath in the Ti-20Zr-6.5Al-4V alloy ratio being decreased was ascribed to two factors: (i) the lamellar α phase was interweaved mutually, as shown from Figure 2, and restrained the growth of other α phases along the longitudinal direction. Consequently, these lamellar α phases grew along the width direction and became thicker; (ii) moreover, certain new α phase precipitated from the parent phase, with specific habit planes and certain orientation relationship with the primary α phase.^[33] As a result, the growth trend of the newly precipitant α phases was restricted along the longitudinal direction and tended to grow along the transverse direction.

B. Coefficient of Friction and Wear Volume

Figures 3(a) through (c) reveal the COF of Ti-20Zr-6.5Al-4V alloy sliding at various velocities at different annealing temperatures. The COF values were all ranged from 0.3 to 0.48 at various sliding velocities.

For each given sliding velocity, the coefficient increased as the normal load increased. The real contact surface and deformation state could influence the frictional force during dry sliding tests.^[34] With increasing normal load, the plastic strain sufficiently increase to trigger the occurrence of delamination. The theory that was firstly proposed by Suh supposed that, during the sliding tests, the contact asperities suffered from an incremental plastic deformation, which could accumulate during repeated sliding contact. When the accumulated strain exceeded a critical level, the cracks may nucleate in the subsurface and then propagate parallel to the surface up to a certain condition.^[35] As a consequence, the COF increased with the normal load. Interestingly, the COF did not increase with sliding velocity, and the highest coefficient was obtained at the intermediate sliding velocity of 0.78 m/s. According to the research conducted by Govindarajan,^[36] the experimental conditions was at in the thermal regime (pure slide), and the thermal effect was significant in this study. As presented in Reference 34, the variations in sliding velocities influenced frictional heat, and finally resulted in the COF variations. As the sliding velocity increased, the friction-induced heat also increased according to the equations raised by Lim *et al.*^[37] The increase in flash temperature did not only increase the adhesion strength

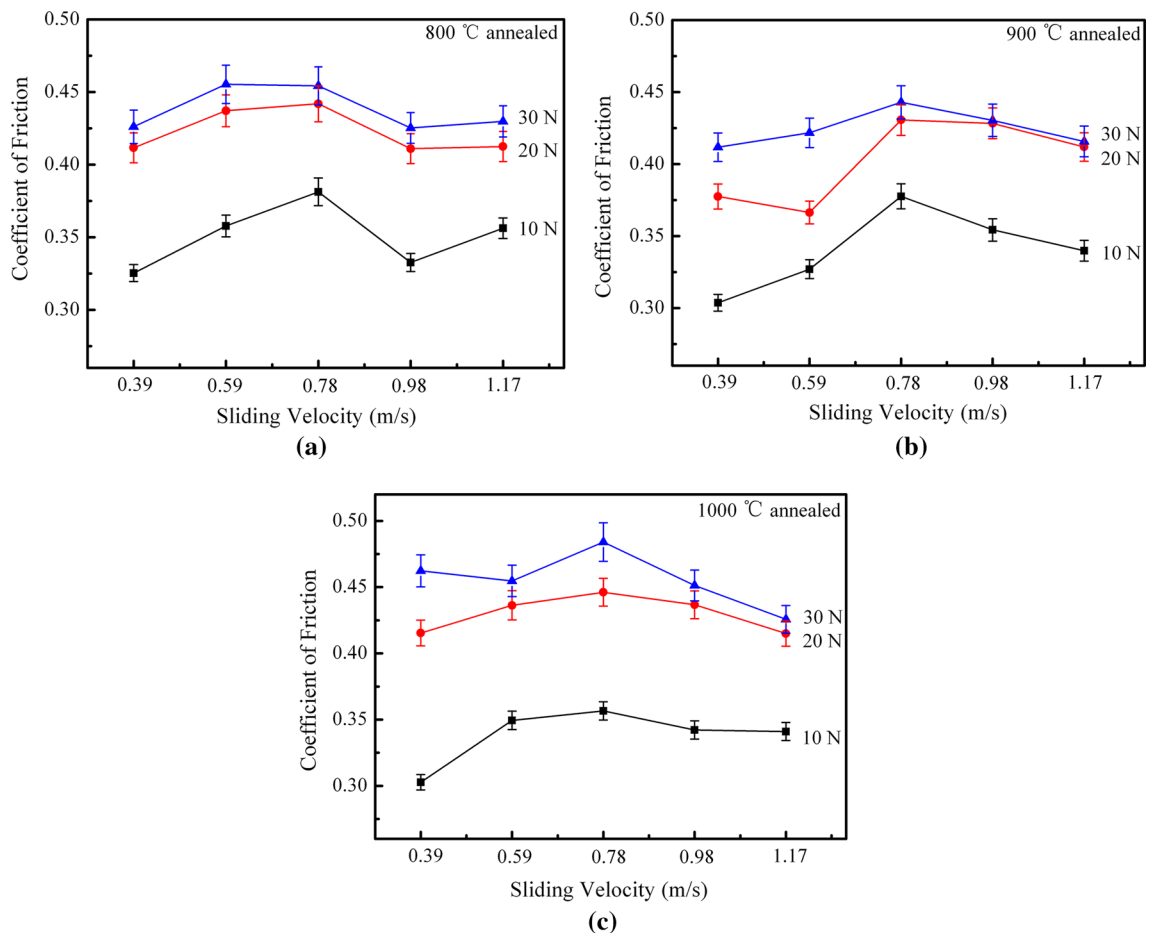


Fig. 3—Coefficient of friction of Ti-20Zr-6.5Al-4V alloy tested at various sliding velocity annealed at (a) 1073 K (800 °C), (b) 1173 K (900 °C), and (c) 1273 K (1000 °C).

due to ease of diffusion but also increased the extent of junction growth because of increased plastic deformation.^[38] Similar results could also be seen in the investigation of Basu's *et al.*,^[3] where the COF of C.P. Ti was lower in liquid nitrogen relative to air. They attributed the results to the lower flash temperature in liquid nitrogen. Therefore, the COF increased monotonously at lower sliding velocity (≤ 0.78 m/s). The COF decreased with increasing sliding velocity possibly because of the softer surface caused by the frictional heat. In vacuum, frictional heat hardly dissipated and accumulated on the contact surfaces. The Ti-20Zr-6.5Al-4V alloy presented an evidently lower thermal conductivity (~ 17 W/mK) than that of stainless steel (~ 40 W/mK).^[38] The higher temperature resulted in a softer TiZrAlV alloy, the shear strength of the asperities on the TiZrAlV alloy decreased and the frictional force became relatively lower. Botto investigated the tribological properties of CoCrTaAlY coating and similar COF variations were illustrated.^[39] The temperature change between the sliding couple originated from the variations of the sliding velocity, and it influenced the COF of TiZrAlV alloy with two effects: (1) on one hand, the COF increased as the modulus of elasticity decreased due to increasing temperature, (2) while on the other

hand the COF decreased as the ultimate shear stress declined. There existed a balance of these two opposite effects, and it could explain the trend of the COF. Consequently, the COF increased with the sliding velocity and reached the maximum value at the sliding

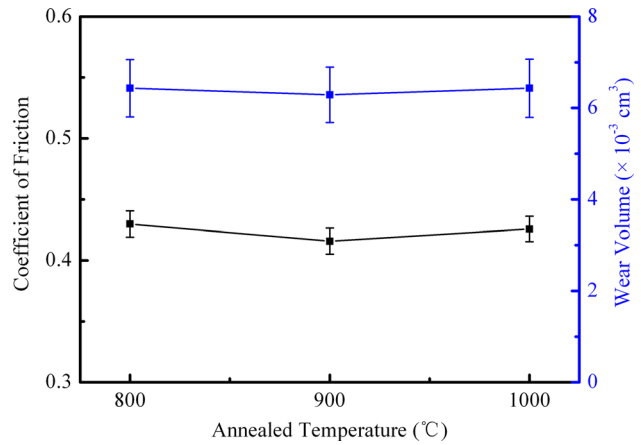


Fig. 5—Coefficient of friction and wear volume of Ti-20Zr-6.5Al-4V alloy annealed at different temperatures tested under 30 N and 1.17 m/s condition.

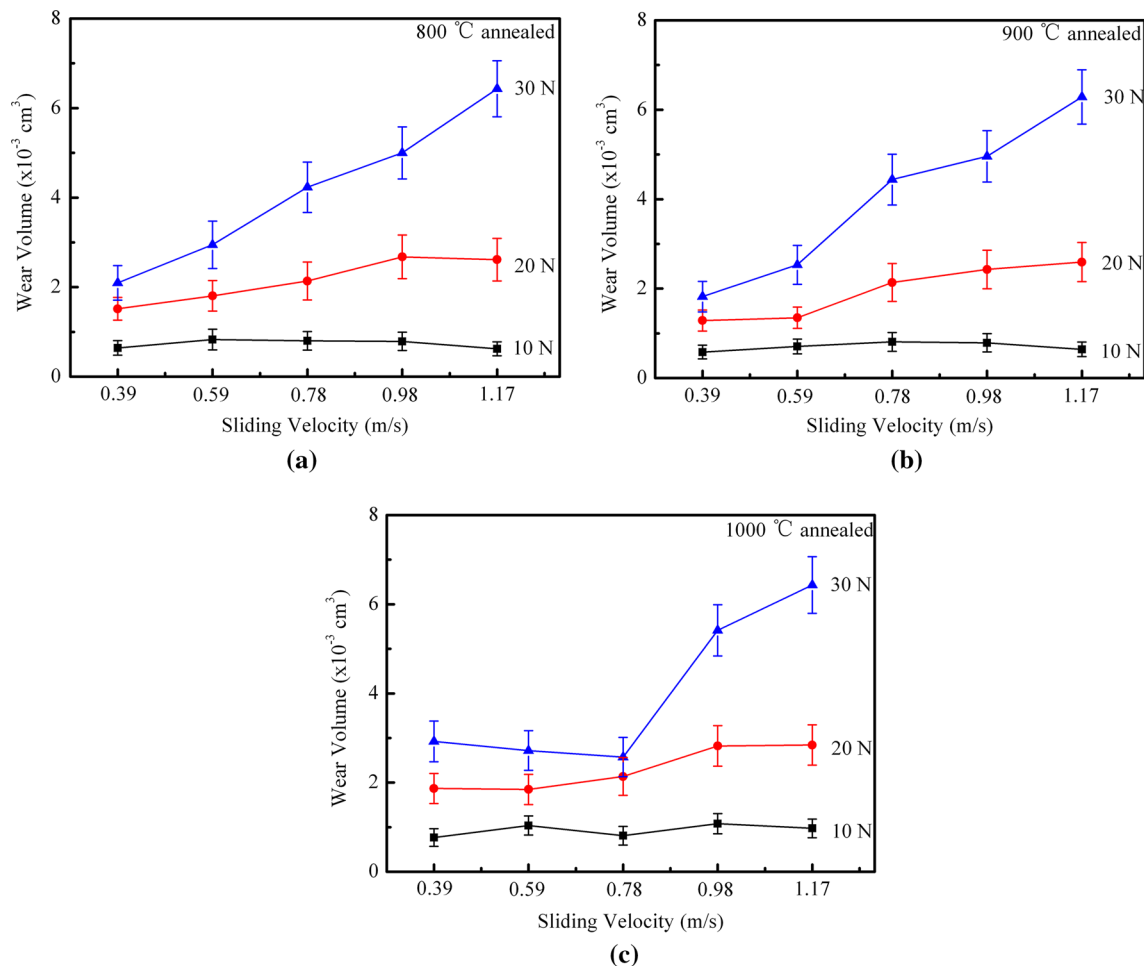


Fig. 4—Wear volume of Ti-20Zr-6.5Al-4V alloy tested at various sliding velocity annealed at (a) 1073 K (800 °C), (b) 1173 K (900 °C), and (c) 1273 K (1000 °C).

velocity of 0.78 m/s, and then the COF decreased with the sliding velocity further increased.

Figures 4(a) through (c) show the curves of the wear volume of Ti-20Zr-6.5Al-4V alloy discs at various

sliding velocities after being annealed at 1073 K, 1173 K, and 1273 K (800 °C, 900 °C, and 1000 °C), respectively. At a certain sliding velocity, the wear volume of the TiZrAlV alloy increased with increasing

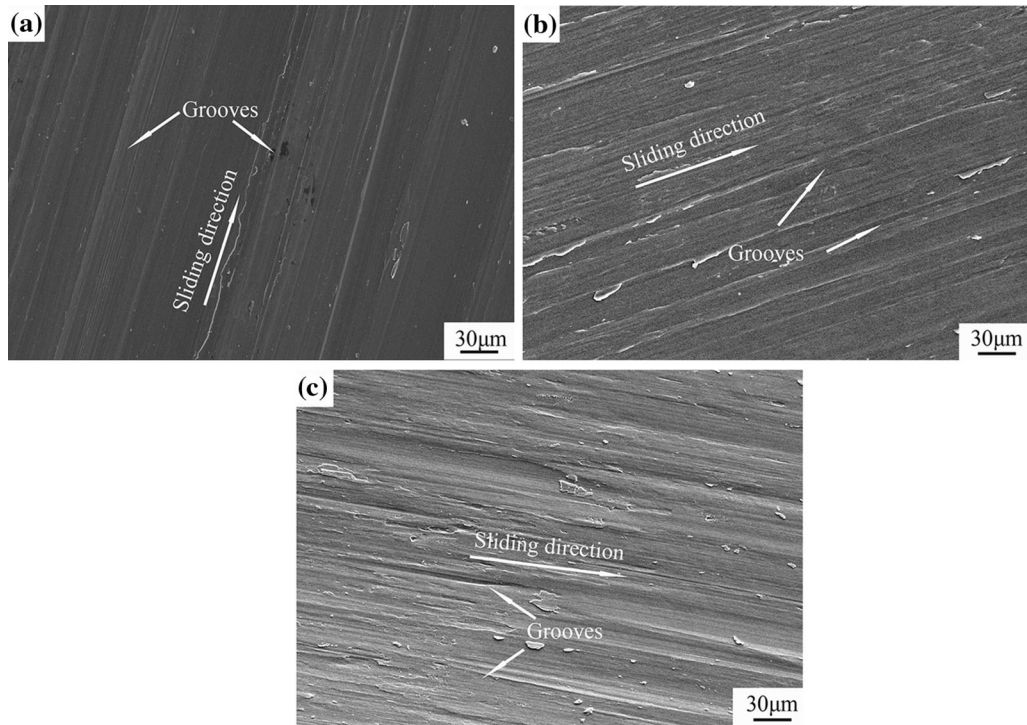


Fig. 6—Wear track of the samples annealed at 1073 K (800 °C) tested under 10 N condition sliding at (a) 0.39 m/s, (b) 0.78 m/s, and (c) 1.17 m/s, respectively.

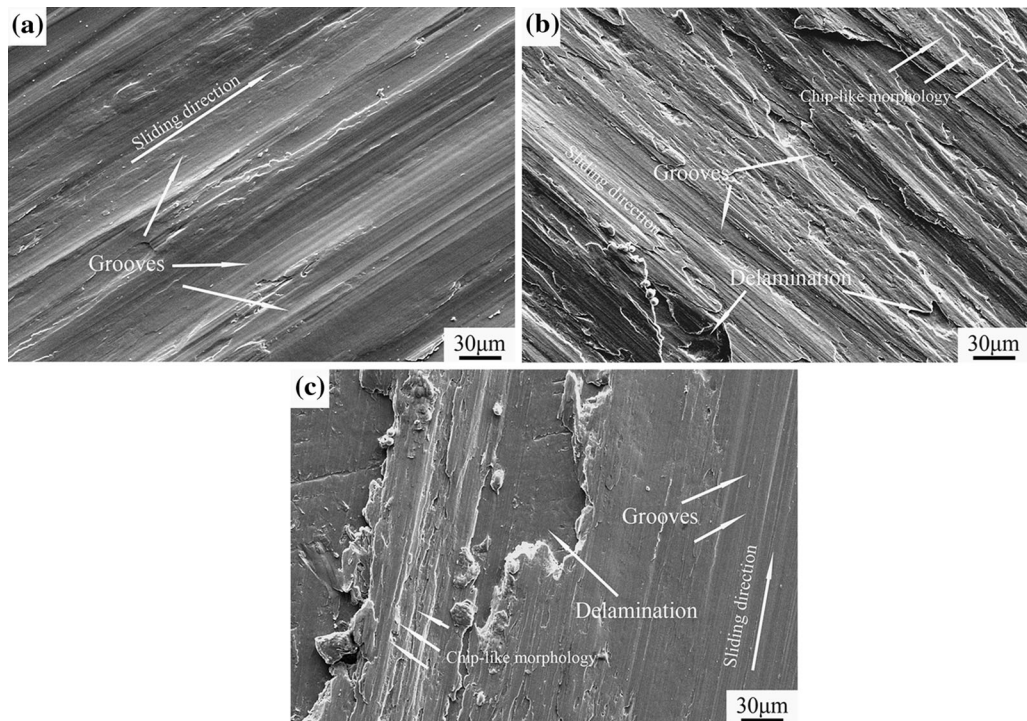


Fig. 7—Wear track of the samples annealed at 1073 K (800 °C) tested under 30 N condition sliding at (a) 0.39 m/s, (b) 0.78 m/s, and (c) 1.17 m/s, respectively.

normal load irrespective of the annealing temperature. Under a low normal load of 10 N, the wear volume of the TiZrAlV alloy slightly changed with increasing sliding velocity. When the normal load increased, the wear volume evidently increased with the sliding velocity. The variations in wear volume at various velocities could be attributed to the wear mechanisms shown below. Under lower normal load (Figure 6), mild abrasive wear was the main wear mechanism. When the normal load increased to 30 N, as shown in Figure 7, the wear became more severe, and delamination became the dominant wear mechanism.

For evaluation of the effect of annealing temperature on the tribological properties of the Ti-20Zr-6.5Al-4V alloy, the COF and wear volume under the normal load of 30 N at the sliding velocity of 1.17 m/s are shown in the Figure 5. The variation of tribological performance slightly changed. As previously investigated,^[26] the results were attributed to similar microhardness values and elastic moduli, indicating that after being annealed

at different temperatures, the samples possessed virtually identical resistance to deformation during sliding.

C. Wear Mechanisms

Figure 6 presents the wear track of the Ti-20Zr-6.5Al-4V alloy annealed at 1073 K (800 °C) under the normal load of 10 N at various sliding velocities. Figure 6(a) shows the wear morphology at the lowest sliding velocity of 0.39 m/s. The shallow grooves on the wear track indicated that the mild abrasive wear was the main wear mechanism. With increasing sliding velocity, the shallow grooves remained the main morphology, revealing that mild abrasive wear was dominant. These results agreed with the wear volumes shown in Figure 4.

Under a high normal load (30 N), the wear tracks of Ti-20Zr-6.5Al-4V alloy sliding at various velocities are illustrated in Figure 7. At the velocity of 0.39 m/s, the deep grooves along the sliding direction indicated that abrasive wear was the main wear mechanism. When the

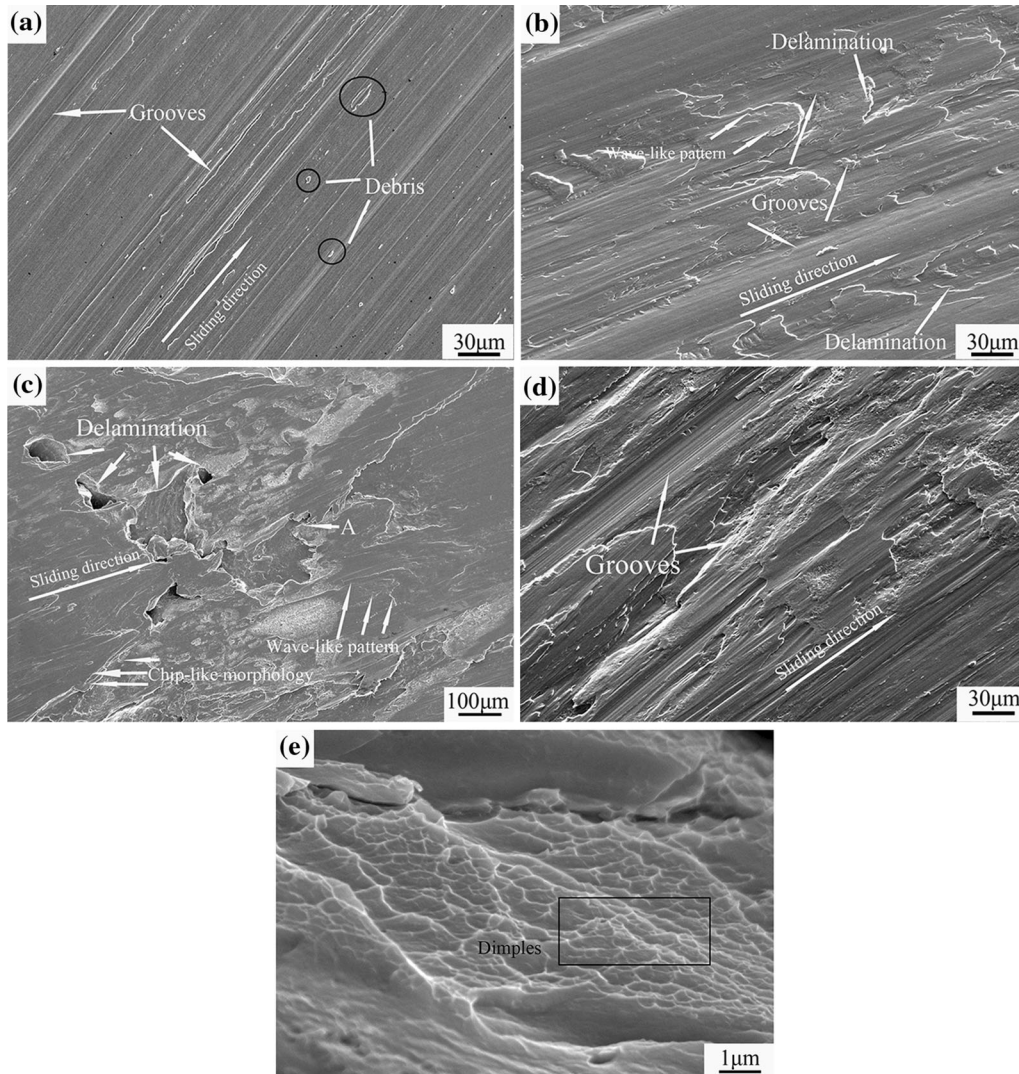


Fig. 8—Morphology of the worn surface tested under (a) 10 N, (b) 20 N, (c) and (d) 30 N with 1273 K (1000 °C) annealed, (e) showing the high magnification view of the location “A” in (c).

sliding velocity was increased to 0.78 m/s, delamination was discovered on wear tracks, indicating that mild delamination wear was a dominant wear mechanism in addition to grooves at this sliding velocity. Moreover, a chip-like morphology was observed on the worn surface,

suggesting that severe plastic deformation occurred during dry sliding. When the sliding velocity was increased to 1.17 m/s, large flaky material was peeled off, and severe delamination was presented. The chip-like morphology indicated that severe plastic

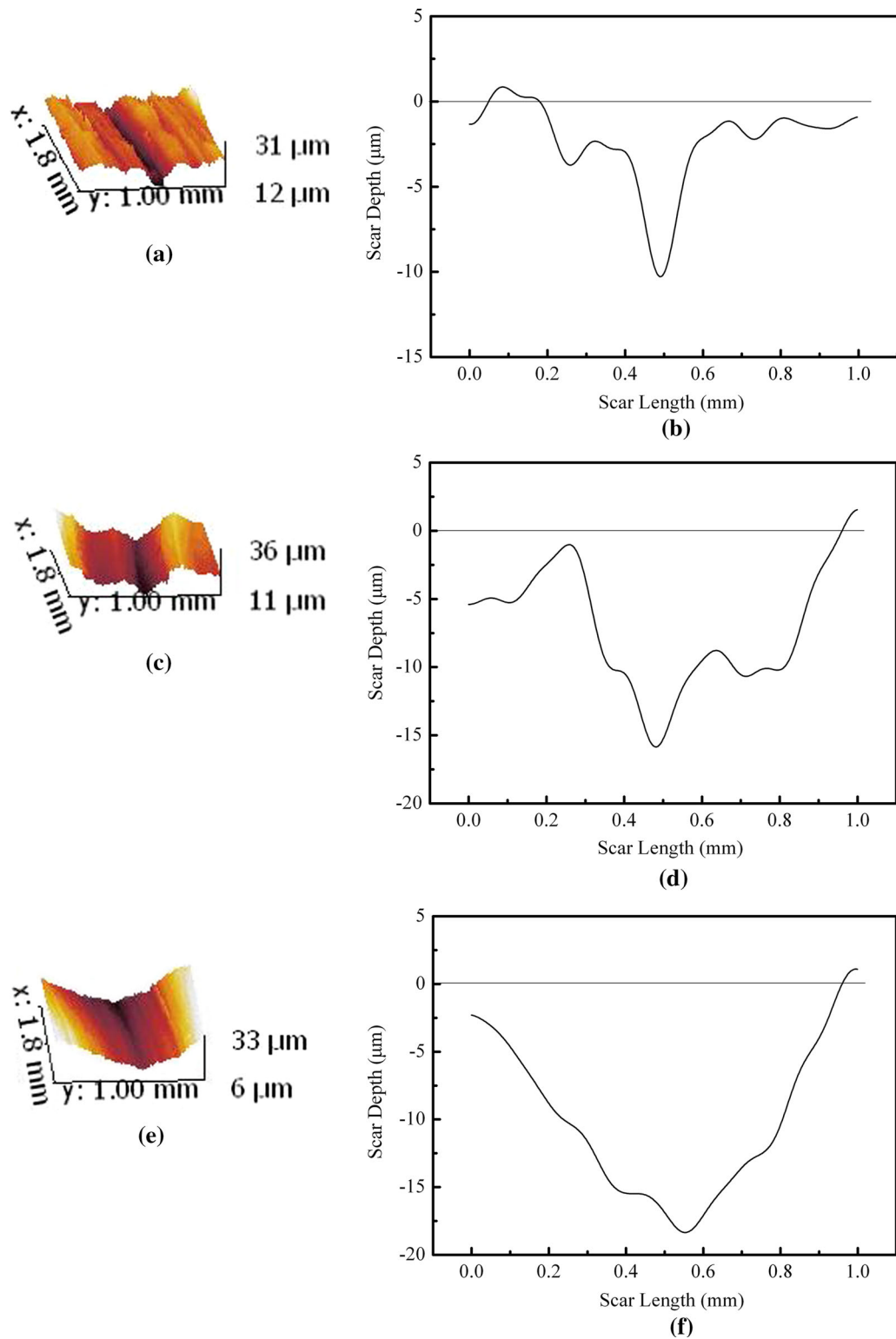


Fig. 9—3D view of the wear scar under (a) 0.39 m/s, (c) 0.78 m/s, (e) 1.17 m/s under the normal load of 30 N; (b, d, f) were the corresponding two-dimensional wear scar.

deformation was also observed on the wear tracks. As shown in Figure 3, the COF of the annealed Ti-20Zr-6.5Al-4V alloy was increased at lower sliding velocity, reaching the maximum value at 0.78 m/s, and then decreased with further increase in velocity, by contrast, the wear rates monotonously increased with sliding velocity. The wear mechanisms may also cause the variations in COF and wear rates. At lower sliding velocities from 0.39 to 0.78 m/s, abrasive wear was dominant, and the particles generated by dry sliding will plough the surface and induce the COFs to increase under these conditions. As the sliding velocities continually increased, plastic deformation became intensive which was similar to the results presented in Reference 40. The researchers ascribed this finding to the increased dislocation density inside the fragments and the extent of boundary misorientation,^[41] then, the ultra-fine microstructure with high density dislocations was generated.^[42] Thus, the COF decrease was possibly attributed to the ultra-fine microstructure formation. Meanwhile, delamination wear was more severe compared with the wear morphology shown in Figure 7, and the wear volumes were monotonously increased along with the sliding velocities.

The wear tracks of Ti-20Zr-6.5Al-4V alloy discs annealed at 1273 K (1000 °C) tested under various normal loads in vacuum is presented in the Figure 8. Figure 8(a) shows the morphology of the worn surface of the annealed samples subjected to a normal load of 10 N. At the lowest applied load, the dominant wear mechanisms were abrasive and mild adhesive wear. Under this condition, the apparent grooves were the main features of surface morphology as presented in the figure. Wear debris was scattered around the grooves generated during dry sliding test. The friction resistance of the surfaces gradually decreased during the experiment, eventually a certain amount of material would peel off. Then, the peeled-off material was crushed and participated during the dry sliding as an abrasive third body. When the normal load was increased to 20 N, deeper grooves and piled up material were observed on the worn surface, as indicated in Figure 8(b). The features were similar to the results previously reported^[12] and were produced by the removal of surface metallic scales. In addition, delamination occurred because of poor dissipation of frictional heat in vacuum and lower thermal conductivity of the Ti-20Zr-6.5Al-4V alloy. The accumulated heat on the surface region decreased the surface strength. Thus, the surface could easily be delaminated from the surface and piled up material could also be observed. The wave-like pattern in Figure 8 indicates the occurrence of plastic deformation. Under the highest load of 30 N condition [Figures 8(c) and (d)], severe delamination occurred. In particular, a chip-like morphology was detected on the edge of the delamination area. This finding was in agreement with the results reported by Farokzadeh *et al.*^[43] This morphology was characteristic for regions subjected to severe wear, with large-scale metallic plates having been ripped and peeled off. Figure 8(e) shows the magnifications of the regions marked by “A” in Figure 8(c). The apparent dimples present proved that

severe plastic deformation was one of the main wear mechanisms in this case besides severe delamination.

D. Topology of the Wear Tracks

In order to reveal the topologies of the wear tracks on the Ti-20Zr-6.5Al-4V discs sliding at various sliding velocities, 3D images of the wear tracks under the normal load of 30 N are displayed in Figure 9. As shown in Figure 9(a), numerous relatively shallow and narrow valleys at the sliding velocity of 0.39 m/s were observed. With increasing the sliding speeds, the valleys became fewer and deeper than those at the lowest sliding velocity, and finally, one deeper and boarder groove was observed at 1.17 m/s, indicating that severe delamination occurred under this condition. Figures 9(b), (d), and (f) show the corresponding two-dimensional topologies in Figures 9(a), (c), and (e), respectively. These images more intuitively show that the wear tracks became deeper with fewer grooves. These topologies could be attributed to the wear mechanisms when tested under different sliding velocities. Under the sliding velocity of 0.39 m/s, numerous shallow and narrow grooves are presented in Figure 7(a). When the sliding speed increased to 1.17 m/s, delamination wear became predominant, and surface peeling-off occurred, consequently, the wear track became deeper and broader as presented in Figure 9(c).

IV. CONCLUSIONS

The effects of the sliding velocities on the vacuum tribological properties of annealed Ti-20Zr-6.5Al-4V and the AISI 440C steel tribo-pair with a ball-on-disc configuration were investigated in this work. The major results were as follows:

1. The coefficient of friction of the annealed Ti-20Zr-6.5Al-4V alloy sliding against AISI 440C steel at various sliding velocities ranged from 0.3 to 0.48. The COF initially increased with the velocity, reached a maximum value at the sliding velocity of 0.78 m/s, and then decreased with further increase in velocity. The wear volumes of the Ti-20Zr-6.5Al-4V alloy increased monotonically with the sliding velocities.
2. Under a lower normal load, the sliding velocity influenced the wear mechanisms insignificantly. With the increase to a higher normal load, the sliding velocities had an obvious effect on wear mechanisms of the Ti-20Zr-6.5Al-4V alloy. Under the lower sliding velocity of 0.39 m/s, abrasive wear was indentified as the main wear mechanism. As the velocity increased, delamination wear and plastic deformation was also observed besides severe abrasive wear. At the highest sliding velocity of 1.17 m/s, the severer abrasive wear accompanied with severe delamination and plastic deformation was the dominant wear mechanisms. The topologies results demonstrated that the grooves become deeper and wider as the sliding velocity increased.

- At the sliding velocity of 1.17 m/s, abrasive and mild adhesive wear were the predominant wear mechanisms of the TiZrAlV alloy annealed at 1273 K (1000 °C) under the normal load of 10 N. With increasing the normal load to 30 N, the main wear mechanisms were severe plastic deformation and delamination wear.

ACKNOWLEDGMENTS

The research was supported by NSFC (Grant No. 51671166/51531005/51571174), National Science Foundation for Distinguished Young Scholars for Hebei Province of China (Grant No. E2016203376).

NOMENCLATURE

DSC	Differential Scanning Calorimetry
OM	Optical Microscopy
XRD	X-ray Diffractometer
SEM	Scanning Electron Microscopy
3D	Three Dimensional
<i>L</i>	Length
<i>W</i>	Width
COF	Coefficient of friction

REFERENCES

- H. Zhong, J. Chen, L.Y. Dai, Y. Yue, B.A. Wang, X.Y. Zhang, M.Z. Ma, and R.P. Liu: *Wear*, 2016, vols. 346–347, pp. 22–28.
- H. Dong and T. Bell: *Wear*, 1999, vols. 225–229, pp. 874–84.
- B. Basu, J. Sarkar, and R. Mishra: *Metall. Mater. Trans. A.*, 2009, vol. 40A, pp. 472–80.
- A. Pauschitz, M. Roy, and F. Franek: *Tribol. Int.*, 2008, vol. 41, pp. 584–602.
- J. Pena, J.M. Guilemany, and F.J. Gil: *Metall. Mater. Trans. A.*, 2006, vol. 37A, pp. 1175–81.
- M.C.M. Farias, R.M. Souza, A. Sinatora, and D.K. Tanaka: *Wear*, 2007, vol. 263, pp. 773–81.
- M.O. Alam and A.S.M.A. Haseeb: *Tribol. Int.*, 2002, vol. 35, pp. 357–62.
- X.X. Li, Y. Zhou, Y.X. Li, X.L. Ji, and S.Q. Wang: *Metall. Mater. Trans. A.*, 2015, vol. 46A, pp. 4360–68.
- S. Asadi Kouhanjani, A. Zarebidaki, and A. Akbari: *J. Alloys Compd.*, 2009, vol. 486, pp. 319–24.
- H. Zhong, L. Dai, Y. Yue, B. Wang, X. Zhang, C. Tan, M. Ma, and R. Liu: *Mater. Sci. Technol.*, 2016, vol. 32, pp. 275–81.
- P.J. Tao, Y.Z. Yang, and Q. Ru: *J. Alloys Compd.*, 2010, vol. 492, pp. L36–39.
- G. Straffelini and A. Molinari: *Wear*, 1999, vol. 236, pp. 328–38.
- R.R. Boyer: *J. Metals.*, 1992, vol. 44, p. 23.
- G. Lutjering and J.C. Williams: *Titanium*, 2nd ed., Springer, Heidelberg, 2007, p. 8.
- M. Vanderhastan, L. Rabert, and B. Verlinden: *J. Mater. Eng. Perform.*, 2007, vol. 16, pp. 208–12.
- A. Molinari, G. Straffelini, B. Tesi, and T. Bacci: *Wear*, 1997, vol. 208, pp. 105–12.
- J. Qu, P.J. Blau, T.R. Watkins, O.B. Cavin, and N.S. Kulkarni: *Wear*, 2005, vol. 258, pp. 1348–56.
- N. Chelliah and S.V. Kailas: *Wear*, 2009, vol. 266, pp. 704–12.
- EHKT Technologies: Opportunities for low cost titanium in reduced fuel consumption, improved emission, and enhanced durability heavy-built vehicles. Oak Ridge National Laboratory Report, ORNL/Sub/4000013062/1, Oak Ridge, TN, 2002.
- R. Jing, S.X. Liang, C.Y. Liu, M.Z. Ma, X.Y. Zhang, and R.P. Liu: *Mater. Sci. Eng. A.*, 2012, vol. 552, pp. 295–300.
- R. Jing, S.X. Liang, C.Y. Liu, M.Z. Ma, and R.P. Liu: *Mater. Des.*, 2013, vol. 52, pp. 981–86.
- Y.H. Yang, C.Q. Xia, Z.H. Feng, X.J. Jiang, B. Pan, X.Y. Zhang, M.Z. Ma, and R.P. Liu: *Corros. Sci.*, 2015, vol. 101, pp. 56–65.
- R. Jing, S.X. Liang, C.Y. Liu, M.Z. Ma, and R.P. Liu: *Mater. Sci. Eng. A.*, 2013, vol. 559, pp. 474–79.
- R. Jing, C.Y. Liu, M.Z. Ma, and R.P. Liu: *J. Alloy Comp.*, 2013, vol. 552, pp. 202–07.
- H.M. Briscoe: Why space tribology *Tribol. Int.*, 1990, vol. 23, pp. 67–74.
- H. Zhong, L.Y. Dai, Y. Yue, B. Zhang, Z.H. Feng, X.Y. Zhang, M.Z. Ma, T. Khosla, J. Xiao, and R.P. Liu: *Tribol. Int.*, 2017, vol. 109, pp. 571–77.
- J. Cheng, J.Q. Ma, Y. Yu, L.C. Fu, Z.H. Qiao, J. Yang, J.S. Li, and W.M. Liu: *J. Tribol.*, 2014, vol. 136, pp. 021604-1–7.
- ASTM G99-05 (Reapproved 2010): Standard test method for wear testing with pin-on-disk apparatus.
- X.X. Li, Q.Y. Zhang, Y. Zhou, J.Q. Liu, K.M. Chen, and S.Q. Wang: *Tribol. Lett.*, 2016, vol. 61, pp. 1–14.
- L. Wang, X.X. Li, Y. Zhou, Q.Y. Zhang, K.M. Chen, and S.Q. Wang: *Tribol. Int.*, 2015, vol. 91, pp. 246–57.
- G. Gautam, N. Kumar, A. Mohan, R.K. Gautam, and S. Mohan: *Tribol. Int.*, 2016, vol. 97, pp. 49–58.
- S.Q. Chen: *Metallography of Titanium Alloys*, National Defence Industry Press, Beijing, 1986.
- G.C. Obasi, S. Biroscas, F.J. Quinta, and M. Preuss: *Acta. Mater.*, 2012, vol. 60, pp. 1048–58.
- S.Z. Wen and P. Huang: *Principles of Tribology*, 2nd ed., Tsinghua University Press, Beijing, 2002, p. 284.
- Fundamental of Friction and Wear of Materials*, 2nd ed., N.P. Suh, and D.A. Rigney, eds., *Fundamental of Friction and Wear of Materials*, ASM, Materials Park, OH, 1980.
- N. Govindarajan and R. Gnanamoorth: *J. Tribol.*, 2008, vol. 130, pp. 041602-1–10.
- S.C. Lim and M.F. Ashby: *Acta Metall.*, 1987, vol. 35, pp. 1–24.
- H. Dong: *Surface Engineering of Light Alloys*, Woodhead Publishing Ltd, Cambridge, 2010.
- D. Botto and M. Lavella: *Wear*, 2014, vol. 318, pp. 89–97.
- Y. Liu, D.Z. Yang, S.Y. He, and W.L. Wu: *Nonferrous Met. Soc. China*, 2003, vol. 13, pp. 1137–40.
- V. Panin, A. Kolubaev, S. Taravov, and V. Popov: *Wear*, 2001, vol. 249, pp. 860–67.
- Y. Liu, D.Z. Yang, S.Y. He, and W.L. Wu: *Mater. Charact.*, 2003, vol. 50, pp. 275–79.
- K. Farokhazadeh and A. Edrissy: *Tribol. Int.*, 2016, vol. 94, pp. 98–111.